

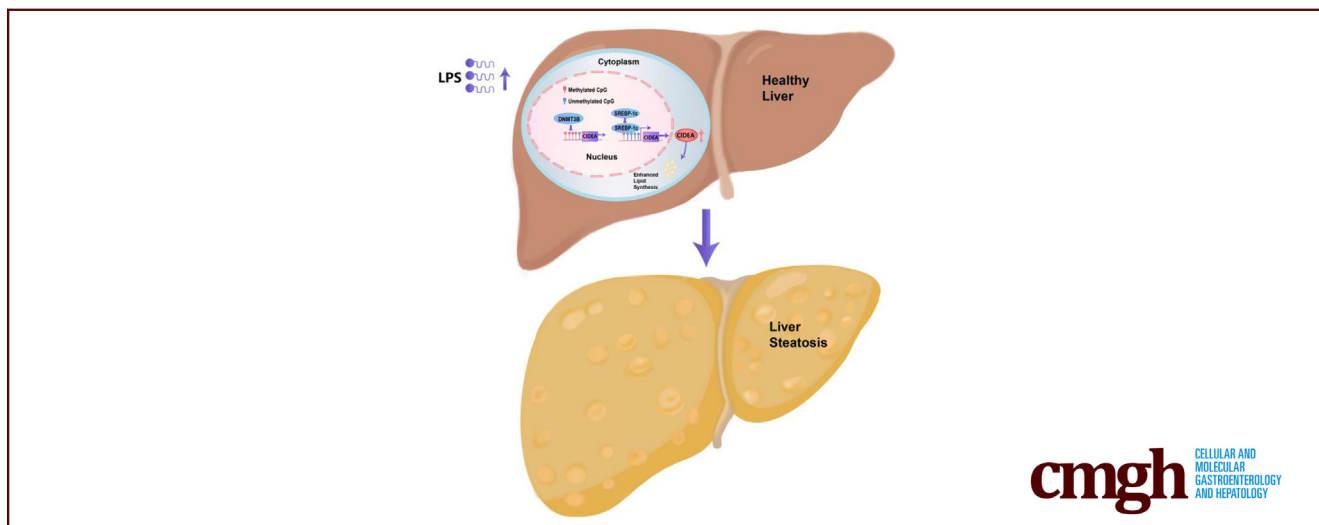
ORIGINAL RESEARCH

DNMT3B Alleviates Liver Steatosis Induced by Chronic Low-grade LPS via Inhibiting CIDEA Expression



Qiang Li,^{1,3,*} Wenjing Wang,^{1,*} Feifan Duan,^{1,*} Yaju Wang,¹ Shuya Chen,¹ Kangyun Shi,¹ Yinyin Xia,¹ Xinyu Li,¹ Yu Gao,^{1,2} and Guoquan Liu^{3,4}

¹Department of Cell Biology, School of Life Science, Bengbu Medical College, Anhui, China; ²Bengbu Medical College Key Laboratory of Cancer Research and Clinical Laboratory Diagnosis, Bengbu Medical College, Bengbu, China; ³Anhui Province Key Laboratory of Translational Cancer Research, Bengbu Medical College, Anhui, China; and ⁴Department of Biochemistry and Molecular Biology, School of Laboratory Medicine, Bengbu Medical College, Anhui, China



SUMMARY

This study summarizes the role of lipopolysaccharide in promoting lipogenesis in the liver. Mechanistically, lipopolysaccharide exacerbates hepatic steatosis by reducing DNA methylation, which activates the transcription and expression of CIDEA. Targeting DNA methyltransferases 3B expression represents a promising therapy for hepatic steatosis.

BACKGROUND & AIMS: Nonalcoholic fatty liver disease is the most prevalent chronic liver disease and threats to human health. Gut dysbiosis caused by lipopolysaccharide (LPS) leakage has been strongly related to nonalcoholic fatty liver disease progression, although the underlying mechanisms remain unclear.

METHODS: Previous studies have shown that low-grade LPS administration to mice on a standard, low-fat chow diet is sufficient to induce symptoms of fatty liver. This study confirmed these findings and supported LPS as a lipid metabolism regulator in the liver.

RESULTS: Mechanically, LPS induced dysregulated lipid metabolism by inhibiting the expression of DNA methyltransferases

3B (DNMT3B). Genetic overexpression of DNMT3B alleviated LPS-induced lipid accumulation, whereas its knockdown increased steatosis in mice and human hepatocytes. LPS-induced lower expression of DNMT3B led to hypomethylation in promoter region of CIDEA, resulting in increased binding of SREBP-1c to its promoter and activated CIDEA expression. Hepatic interference of CIDEA reversed the effect of LPS on lipogenesis. These effects were independent of a high-fat diet or high fatty acid action.

CONCLUSIONS: Overall, these findings sustain the conclusion that LPS is a lipogenic factor and could be involved in hepatic steatosis progression. (*Cell Mol Gastroenterol Hepatol* 2024; 17:59–77; <https://doi.org/10.1016/j.jcmgh.2023.09.002>)

Keywords: Liver steatosis; DNMT3B; LPS; CIDEA; DNA methylation.

Hepatic steatosis, also known as fatty liver, is the main symptom of nonalcoholic fatty liver disease (NAFLD). NAFLD has a prevalence of 34% worldwide,¹ and approximately 20% to 27% of patients with NAFLD have nonalcoholic steatohepatitis (NASH), the onset of advanced liver diseases, such as liver fibrosis,² liver cirrhosis,³ and hepatocellular carcinoma.⁴ And NAFLD even raises the

morbidity of type 2 diabetes, cardiovascular diseases, and obesity, which threatens human's health.⁵

Although the mechanism underlying NAFLD pathogenesis is still elusive, growing evidence suggests that microbes are involved in energy homeostasis and NAFLD progression.⁶ The overgrowth of intestinal gram-negative bacteria in patients with NAFLD leads to the accumulation of endotoxin lipopolysaccharides (LPS), which increase serum endotoxemia. Then LPS is localized in hepatocytes and activates inflammation via TLR4, which elicits liver damage and exacerbates NAFLD, causing NASH diseases.⁷ However, a study revealed that low and nonlethal doses of endotoxins increased hepatic lipid storage in rats fed with a chow diet.⁸ Another experimental mouse model revealed that continuous subcutaneous infusion of 300 $\mu\text{g}/\text{kg}/\text{day}$ LPS for 4 weeks significantly increased liver weight and triglyceride (TG) content, even though the mice were fed with chow diet.⁹ Similar results were found in another study where LPS treatment (240 $\mu\text{g}/\text{kg}/\text{day}$) for 2 weeks could trigger liver steatosis in chow diet-fed mice.¹⁰ These studies indicate that aberrant serum LPS increases may be a regulator of lipid metabolism in non-high-fat diet (HFD)-induced hepatic steatosis.

DNA methylation frequently occurs in eukaryotic cells and could regulate gene expression without changing gene sequences, and abnormal DNA methylation is correlated with numerous diseases, including NAFLD. The genome-wide screening of sites has revealed a demethylation tendency of hepatic DNA in patients with NAFLD.¹¹ Clinical research also indicated that global DNA methylation yielded a decreasing trend in liver biopsy specimens of patients with NAFLD with increased fibrosis and inflammation progression.¹² The same analysis of genome-wide DNA methylation suggested HFD induced the hypomethylation of liver lipogenic genes,¹³ which illustrates that the DNA methylation is critical for NAFLD progression. DNA methylation often occurs at the CpG loci of gene promoters and is regulated by 2 types of enzymes: DNA demethylases and DNA methyltransferases (DNMTs). Overall, it is highly conceivable that DNMTs are related to hypomethylation in NAFLD.

Inspired by the previous study, we sought to confirm whether LPS acts as a regulator of lipometabolism in liver even without HFD induction. The integrated transcriptome-metabolome analysis was used to gain novel insights into the novel genes regulating lipid metabolism in mice livers after low-dose LPS treatment. Our study found that DNA methyltransferases 3B (DNMT3B) was downregulated by LPS treatment. DNMT3B repression increased lipid accumulation in oleic acid-pretreated hepatocytes, whereas its overexpression alleviated this effect. Further study found that LPS exerted its role in lipid metabolism via DNMT3B-regulated CIDEA promoter methylation and CIDEA transcription, facilitating TG synthesis and lipid droplet (LD) formation. Overall, our results provided evidence that DNMT3B is involved in LPS-activated liver steatosis progression.

Results

Low Doses of LPS Triggered Hepatic Steatosis

To verify whether LPS contributes to liver steatosis, LPS (300 $\mu\text{g}/\text{kg}/\text{day}$) was continuously infused into mice by a


micro-osmotic pump and subjected to chow diet or HFD (Figure 1A). Although the plasma LPS in chow diet-fed mice was comparable to the HFD-fed mice (Figure 1B), the body weight did not increase compared with those fed with chow diet (Figure 1C). Of note, the liver weight and serum transaminases were higher in LPS-infused mice (Figure 1D–F), whereas no differences were observed for serum TG, serum total cholesterol (TC) (Figure 1G), and oral glucose tolerance test (OGTT) in the chow diet and LPS-treated group (Figure 1H). Low circulating LPS could promote liver steatosis (Figure 1I–K) and IL-1, IL-6, and TNF- α expression in the liver (Figure 1L). The mRNA levels, especially those involved in lipid formation, such as perilipin 2 (PLIN2), perilipin 4 (PLIN4), CIDEA, and CIDEA were significantly increased (Figure 1M). These results suggested that LPS is a lipid metabolism regulator and can induce hepatic steatosis even in chow diet-fed mice.

LPS Altered the Liver Metabolite Profiles in Mice

To assess the metabolic change in mice liver after LPS infusion, liver metabolites were quantified via the ultra-high performance liquid chromatography-quadrupole time-of-flight mass spectrometry (UHPLC-QTOF-MS/MS)-based untargeted metabolomics. One hundred thirty-six metabolites (65 in positive or 71 in negative mode) were identified based on the criteria: fold change >1.5 or <0.5, VIP values >1.0 and *P* values <.05. The volcano plot revealed a total of 108 differentially expressed metabolites after LPS infusion compared with the chow diet group (Figure 2A). Pathway enrichment analysis showed that the identified different metabolites were primary included in glycolysis, glycerolipid, and alanine metabolism (Figure 2B). The top 29 differentially expressed metabolites that contributed to metabolic alterations were visualized in a heatmap (Figure 2C), including carbohydrates, amino acids, long chain fatty acids, and so on. As shown in principal component analysis plots, different clustering of liver samples was found both in negative and positive mode (Figure 2D). Subsequent orthogonal partial least squares discriminant analysis modeling revealed that the chow diet and LPS-treated groups were clearly separated (Figure 2E). The permutation test indicated the prediction ability parameters

*Authors share co-first authorship

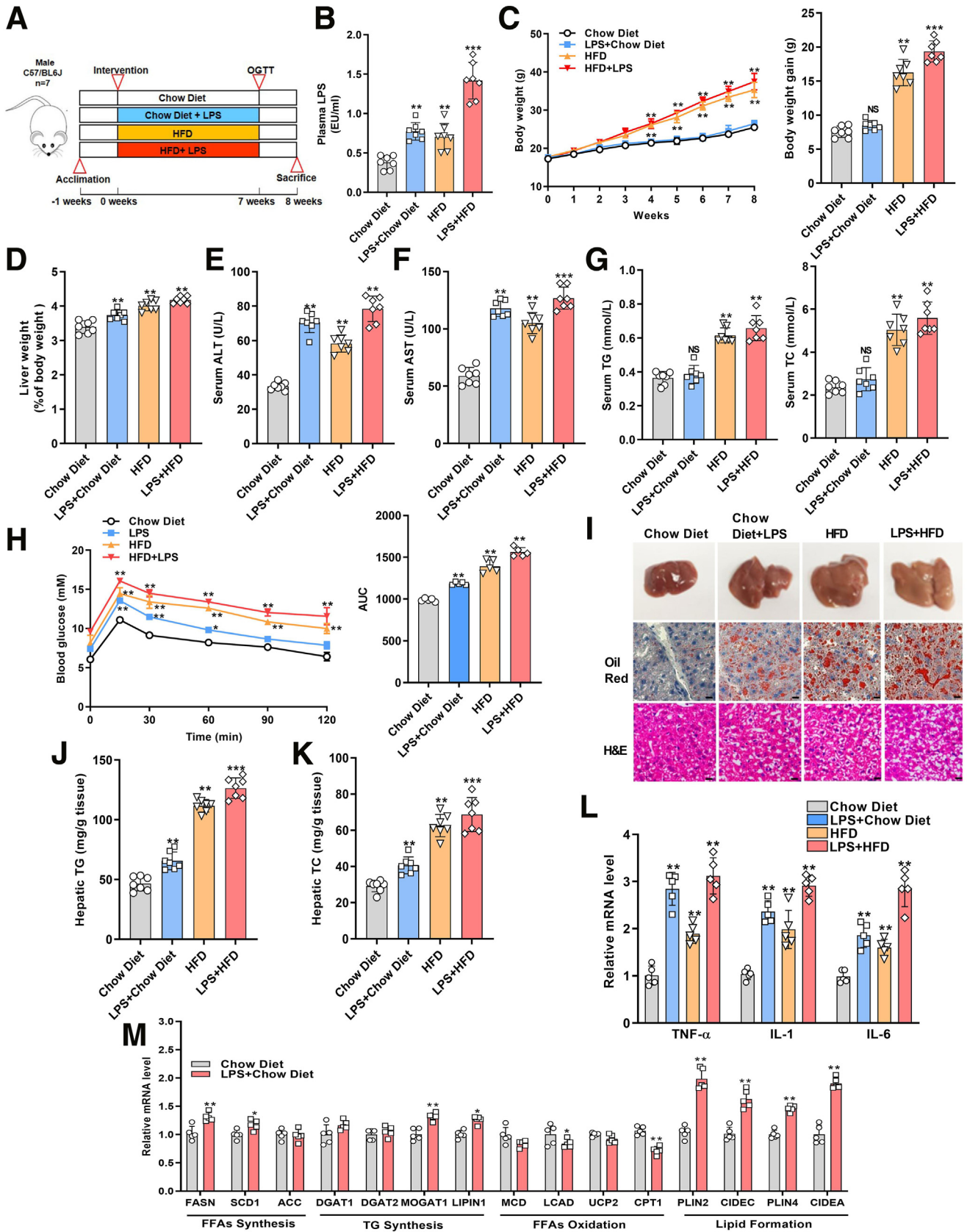
Abbreviations used in this paper: AAV, adeno-associated virus; ALT, alanine transaminase; AST, aspartate transaminase; ChIP, chromatin immunoprecipitation; DNMT, DNA methyltransferase; DNMT3B, DNA methyltransferases 3B; H&E, hematoxylin and eosin; HFD, high-fat diet; KEGG, Kyoto Encyclopedia of Genes and Genomes; LD, lipid droplet; LPS, lipopolysaccharides; MSP, methylation-specific polymerase chain reaction; NAFLD, nonalcoholic fatty liver disease; NASH, nonalcoholic steatohepatitis; OGTT, oral glucose tolerance test; RNAseq, RNA sequencing; TC, total cholesterol; TG, triglyceride; UHPLC-QTOF-MS/MS, ultra-high performance liquid chromatography-quadrupole time-of-flight mass spectrometry.

 Most current article

© 2023 The Authors. Published by Elsevier Inc. on behalf of the AGA Institute. This is an open access article under the CC BY-NC-ND license (<http://creativecommons.org/licenses/by-nc-nd/4.0/>).

2352-345X

<https://doi.org/10.1016/j.jcmgh.2023.09.002>



(Q^2) exceeded 0.5, and the interpretation ability parameters (R^2Y) approached 1.0, suggesting the models exhibited good predictability and reliability (Figure 2F). Next, Kyoto Encyclopedia of Genes and Genomes (KEGG) topology analysis, which based on the differential metabolites, was conducted to find the metabolic pathway enrichment. We found that α -linolenic acid metabolism (impact value = 1.375; $P < .0001$), retinol metabolism (impact value = 1.349; $P < .0001$), glutathione metabolism (impact value = 0.745; $P < .0001$), ascorbate and aldarate metabolism (impact value = 0.949; $P < .001$), and glycerolipid metabolism (impact value = 1.183; $P < .0001$) were significantly enriched metabolic pathways altered by LPS treatment (Figure 2G). Collectively, these results suggest that LPS could change the liver metabolic profiles, including lipid metabolism in the liver.

LPS Increased Lipid Accumulation in Hepatocytes and Reduced DNMT3B Expression

To confirm whether LPS regulated lipid metabolism in hepatocytes, mice primary hepatocytes and human hepatoma carcinoma cell HepG2 were pretreated with oleic acid (100 μ M) and then treated with LPS (500 ng/mL) or oleic acid (100 μ M) or LPS (500 ng/mL) and oleic acid (100 μ M). LPS treatment increased TG content in primary hepatocytes (Figure 3A–B) and HepG2 cells (Figure 3C–D) and aggravated oleic acid-induced TG accumulation. The expression of lipid formation genes (PLIN2, PLIN4, CIDEA, and CIDEA) were markedly augmented after LPS treatment (Figure 3E). RNA sequencing (RNAseq) analysis similarly showed that the expression of PLIN2, PLIN4, CIDEA, and CIDEA was markedly upregulated in LPS-infused mice liver (Fold change >1.5 ; $P < .01$) (Figure 3F). To elucidate the mechanism, the RNAseq data were further analyzed and revealed that LPS down-regulated DNMT3B expression (Fold change <0.5 ; $P < .01$) (Figure 3F). NAFLD is correlated with aberrant DNA methylation.¹¹ Accordingly, DNMT3B might be involved in LPS-induced hepatic steatosis. The dose-dependent effect of LPS on DNMT3B expression in cells was analyzed to validate this conclusion. Five hundred ng/mL LPS could effectively decrease DNMT3B expression in hepatic cells (Figure 3G–H). Additionally, microarray data from the National Center for Biotechnology Information (accession nos. GDS4881) revealed that there was no difference in DNMT3B level among NAFLD or NASH and patients with NAFLD and healthy people (Figure 3J). These results

indicated that LPS could facilitate TG synthesis, and DNMT3B might be a specific target for LPS.

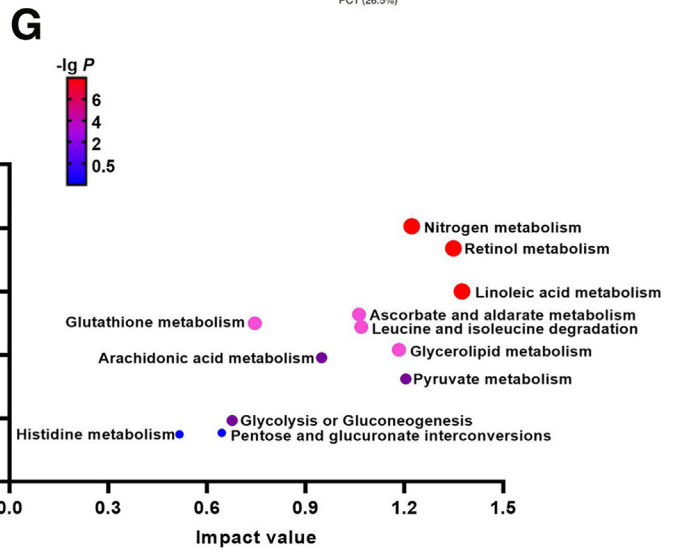
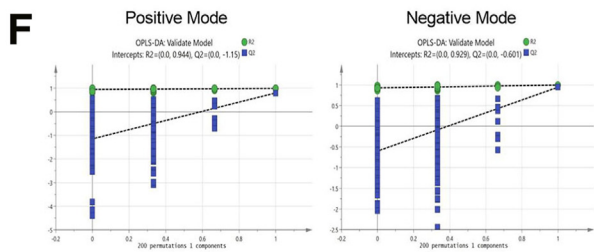
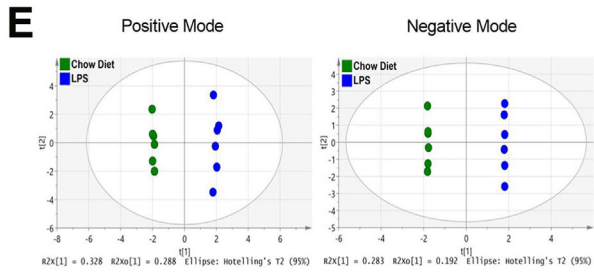
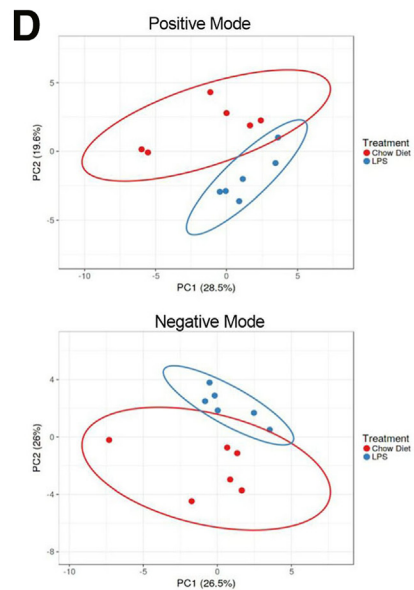
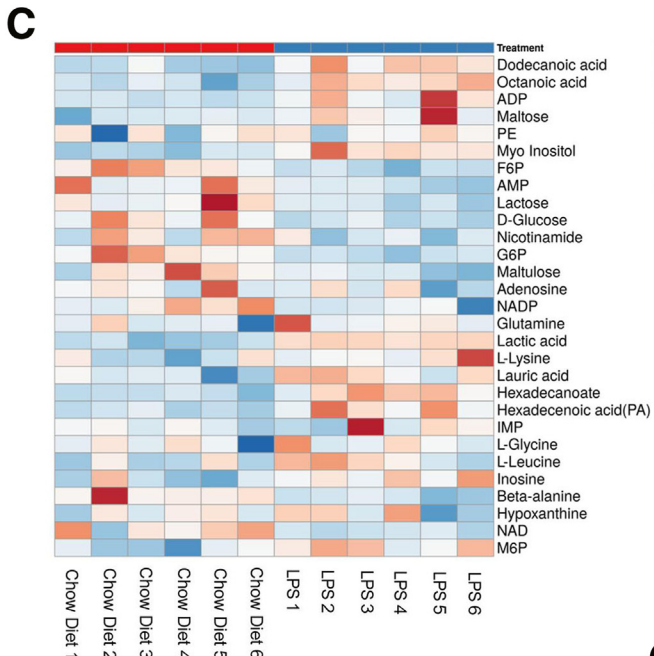
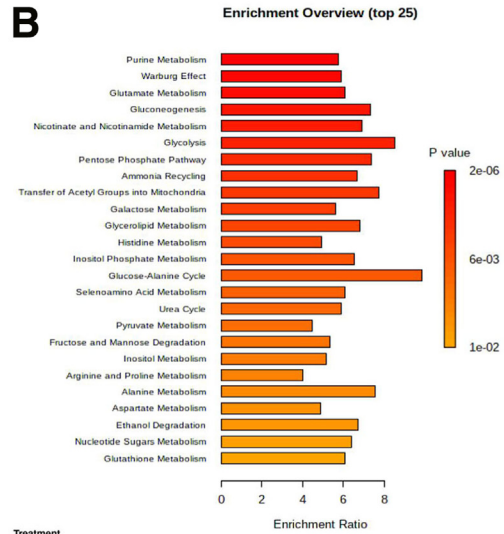
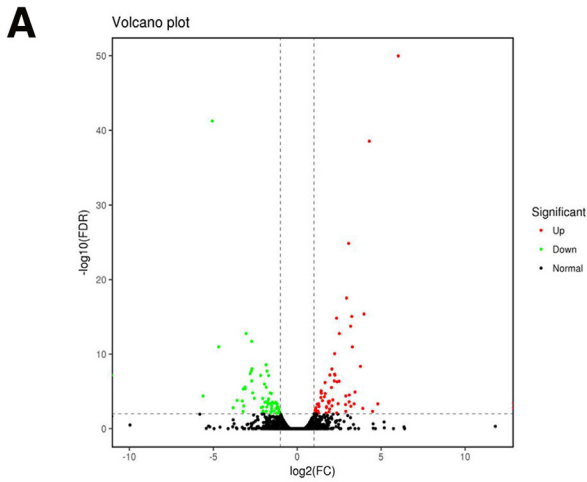
DNMT3B Overexpression Improved LPS-induced Hepatic Steatosis

To evaluate how DNMT3B affect lipid metabolism in LPS-treated hepatic cells, lentiviruses expressing DNMT3B (oeDNMT3B) or empty vector (oeVec) and lentiviruses expressing DNMT3B shRNA (shDNMT3B) or a control shRNA (shNC) were expressed in primary hepatocytes and HepG2 cells. Lentiviruses expressing DNMT3B infection markedly increased DNMT3B expression in primary hepatocytes (Figure 4A). Moreover, DNMT3B overexpression counteracted the effect of LPS on LD formation in oleic acid (100 μ M)-pretreated primary hepatocytes (Figure 4B–C) and HepG2 cells (Figure 4D–F), whereas DNMT3B interference with siRNA in oleic acid-pretreated hepatocytes aggravated this effect in primary hepatocytes (Figure 4G–I). Similarly, DNMT3B silencing augmented LPS-induced lipid accumulation in oleic acid-pretreated HepG2 cells (Figure 4J–L). Finally, ¹⁴C-palmitate was used to detect the rate of fatty acid β -oxidation. The primary hepatocytes showed decreased fatty acid β -oxidation after LPS treatment, whereas DNMT3B overexpression reversed this effect (Figure 4M). However, DNMT3B knockdown combined with LPS reduced the rate of fatty acid β -oxidation in primary hepatocytes (Figure 4N). Collectively, these data suggest that LPS promoted TG synthesis in hepatic cells via down-regulating DNMT3B expression.

LPS Promotes CIDEA Expression Via Demethylating Its Promoter

Based on the above results, the murine and human lipogenic genes (PLIN2, PLIN4, CIDEA, and CIDEA), which harbored DNA methylation sites in their promoter region, are essential for LPS-DNMT3B-induced lipogenesis. In silico analysis revealed there is a CpG island ~ 0.05 to 0.25 kb upstream of the murine CIDEA locus and ~ 0.15 to 0.25 kb upstream of the human CIDEA locus, implying CIDEA is a candidate gene (Figure 5A). To determine the exact mechanism, cells were exposed to different concentrations of LPS used to treat. LPS exposure elevated CIDEA expression (Figure 5B–C) but reduced the total 5-mC levels (Figure 5D–E) in a dose-dependent manner. Methylation-specific polymerase chain reaction (MSP) validated that LPS exposure lowered methylation levels within the CIDEA CpG island (Figure 5F). Besides, LPS exposure significantly

Figure 1. (See previous page). **Effect of low dose LPS on liver steatosis in mice.** C57BL/6 mice (male) were access to HFD or chow diet for 8 weeks and infused with LPS (300 μ g/kg/day) continuously during the first 4 weeks through a micro-osmotic pump. (A) Schematic representation of animal experiment design. Serum LPS concentration (B), body weight (C), liver weight (D), ALT (E), and AST (F), as well as TG (G) and TC concentration in serum of mice treated as the animal experiment design ($n = 7$). (H) OGTT of food intake in LPS- or HFD-treated mice ($n = 7$). (I) Representative morphology of the livers (upper), Oil Red O staining (middle), and microphotographs of H&E (bottom). Scale bar, 50 μ m. (J–K) Hepatic TG (J) and hepatic TC (K) content were also directly measured ($n = 7$). (L) Liver mRNA levels of inflammatory cytokine genes ($n = 5$). (K) Expression of lipogenic genes in liver ($n = 7$). Values are determined by the Student t -test when the 2 groups were compared. For 3 or more groups comparison, 1-way analysis of variance followed by Newman-Keuls multiple comparison test was used. Data are exhibited as mean \pm standard error of the mean. * $P < .05$; ** $P < .01$; *** $P < .001$.



activated the transcriptional activity of CIDEA promoter in Hepa1-6 cells and HepG2 cells (Figure 5G). Quantitative chromatin immunoprecipitation (ChIP) assays revealed that LPS attenuated the binding of DNMT3B to CIDEA promoter (Figure 5H) and the 5-mC signals (Figure 5J). SREBP-1c is a lipogenesis gene and a well-known transcription factor of CIDEA.¹⁴ We found that knocking down SREBP-1c in Hepa1-6 and HepG2 cells significantly inhibited CIDEA expression (Figure 5J), and LPS increased the accumulation of SREBP-1c in the promoter of CIDEA (Figure 5K). The functional assays showed that CIDEA knockdown with lentiviruses blocked the effect of LPS on lipogenesis in oleic acid (100 μ M)-pretreated primary hepatocytes and HepG2 cells (Figure 5L). These data demonstrate that LPS caused hypomethylation of the CIDEA promoter and facilitated the recruitment of SREBP-1c to increase CIDEA expression.

DNMT3B is Required for LPS-mediated CIDEA Expression

To explore whether LPS induced CIDEA expression through DNMT3B-mediated DNA methylation, primary hepatocytes and HepG2 cells were first infected with lentiviruses expressing DNMT3B or DNMT3B shRNA. When DNMT3B expression was induced in primary hepatocytes or HepG2 cells, it suppressed CIDEA expression and blocked the effect of LPS on CIDEA (Figure 6A). However, DNMT3B knockdown stimulated CIDEA expression and enhanced the effect of LPS on CIDEA expression (Figure 6B). The bisulfite sequencing PCR (BSP) showed that DNMT3B overexpression elevated CpG island methylation, but DNMT3B interference decreased the CpG island methylation in promoter region of CIDEA (Figure 6C–D). Moreover, DNMT3B overexpression upregulated the total 5-mC levels (Figure 6E) and enhanced the binding of DNMT3B to CIDEA promoter and 5-mC signals in Hepa1-6 cells and HepG2 cells (Figure 6F–G). Further reporter gene assays revealed that the CIDEA promoters were deactivated by DNMT3B overexpression (Figure 6H). Moreover, CIDEA interference partially prevented the effect of LPS plus DNMT3B-induced lipogenesis (Figure 6I–J). These results provide compelling evidence that LPS-induced DNMT3B low expression attenuates the methylation level in the CIDEA promoter and increases CIDEA expression, promoting lipogenesis in vitro.

AAV8-DNMT3B Ameliorates Hepatic Steatosis in LPS-infused Mice

The effect of DNMT3B overexpression on lipid accumulation caused by LPS in vivo was assessed to verify whether the findings have translational significance. C57BL/6 male mice (6-weeks-old) were allocated into 5 groups randomly.

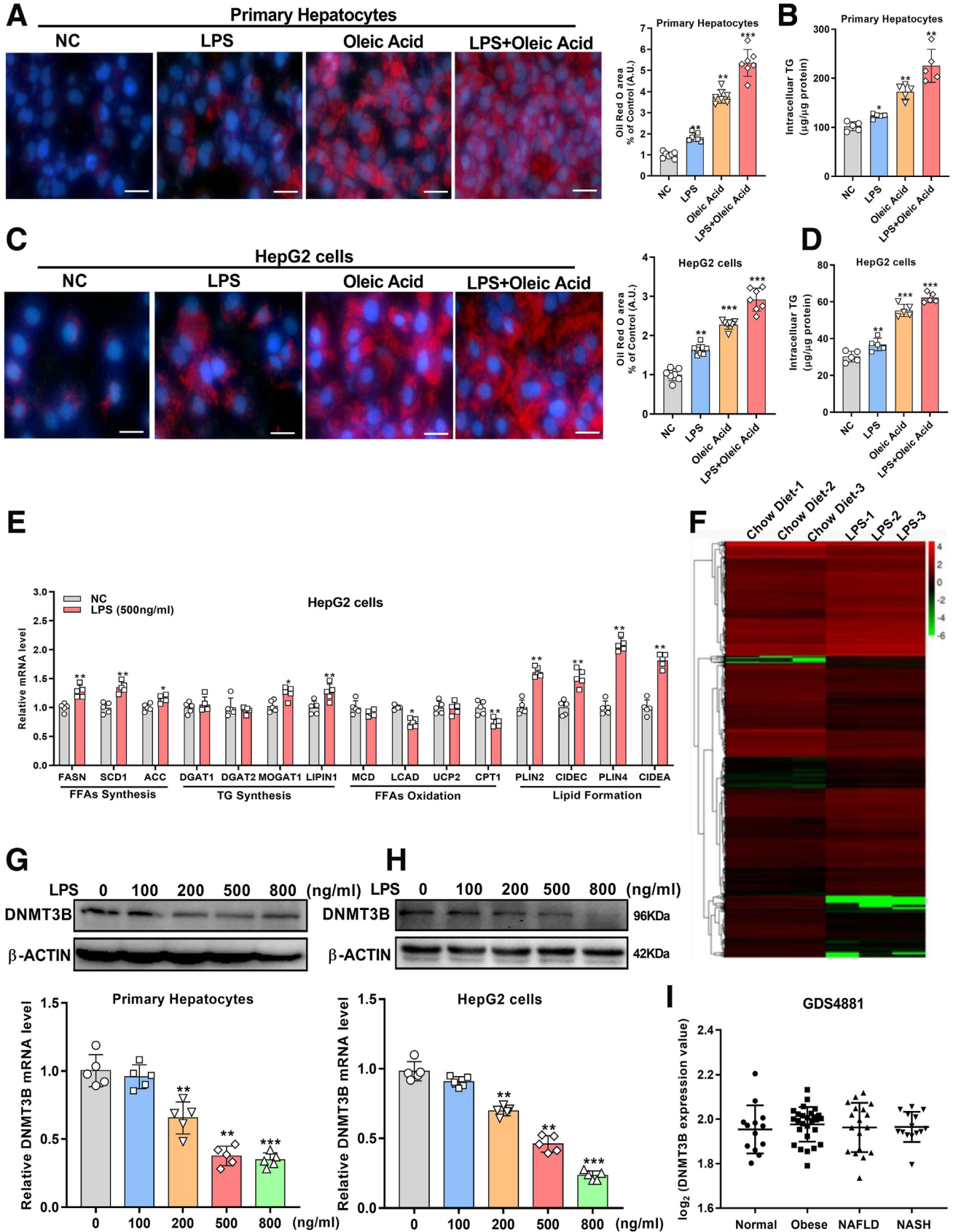
In the first and second groups, mice injected with AAV8-DNMT3B or control via the tail vein were fed for 8 weeks with chow diet plus LPS infusion (LPS-chow diet groups). In the third and fourth groups, mice injected with AAV8-DNMT3B or AAV8-GFP via tail vein were fed with HFD for 8 weeks plus with LPS infusion (LPS-HFD groups). Mice injected with AAV8 control and fed with chow diet were used as the control group. We found that AAV8-DNMT3B injection markedly decreased the body weight of LPS-HFD-administered mice (Figure 7A–B) and liver weight of LPS-chow diet as well as LPS-HFD-administered mice (Figure 7C). AAV8-DNMT3B reduced the serum aspartate transaminase (AST) and alanine transaminase (ALT) levels in LPS-chow diet and LPS-HFD-administered mice (Figure 7D). Besides, AAV8-DNMT3B reduced TG accumulation, degree of liver fibrosis stained with Sirius red (Figure 7E–G) and counteracted the effects of LPS on inflammation biomarkers generation of IL-2, IL-13, IL-1 β , IL-6 and TNF- α in LPS-chow diet and LPS-HFD-treated mice livers. The expression of CIDEA in LPS-chow diet and LPS-HFD-fed mice liver was significantly decreased after DNMT3B overexpression (Figure 7H). Functional assays revealed an increased β -oxidation rate in mice primary hepatocytes (Figure 7I–J) with DNMT3B overexpression.

However, AAV8-shDNMT3B injection markedly increased the body weight of LPS-chow diet-administered mice (Figure 8A–B) and liver weight (Figure 8C). DNMT3B knockdown also increased the serum AST and ALT levels in LPS-chow diet-administered mice (Figure 8D). Besides, DNMT3B knockdown increased TG accumulation (Figure 8E–G), inflammation biomarkers production (Figure 8H), and CIDEA expression (Figure 8I) in the LPS-chow diet-fed mice livers. Finally, the functional assays revealed a decreased β -oxidation rate in mice primary hepatocytes (Figure 8J–K) with DNMT3B knockdown (Figure 8L). Taken together, these data suggest that inducing DNMT3B expression in liver alleviates LPS-induced hepatic steatosis, and DNMT3B represents a potential therapeutic target for abnormal lipid accumulation in the liver induced by LPS.

Discussion

In this study, we identified the role of DNMT3B on lipometabolism in hepatocytes and its correlation with LPS-induced hepatic steatosis, which has been reported before. LPS treatment markedly increased hepatic lipogenesis by repressing DNMT3B expression in oleic acid-pretreated hepatocytes. Functional studies suggested that DNMT3B overexpression significantly reversed the pro-lipogenic effect of LPS on the liver, whereas its silencing exacerbated steatosis induced by LPS. Furthermore, LPS resulted in a

Figure 2. (See previous page). LPS infusion regulates liver metabolite profiles. (A) Metabolomics change presented by volcano plot. (B) KEGG pathway analysis based on the metabolite changes between chow diet and LPS infusion group. (C) Heatmap of 29 significantly changed metabolites between chow diet and LPS infusion group (n = 6). The boxes in orange or blue represent high or low z-score values, respectively. (D–E) Principal component analysis score plots (D) and OPLS-DA scores plots (E) of the liver from the chow diet and LPS infusion group (n = 6). (F) Permutation tests performed in model of OPLS-DA (200 random permutations). The negative mode analysis was also included. (G) Pathway impact in topology analysis. OPLS-DA, Orthogonal partial least squares-discriminant analysis.



reduction in DNA methylation within the promoter of CIDEA, which caused a decrease in DNMT3B recruitment and an increase in SREBP-1c recruitment to the same promoter. Accordingly, CIDEA was abnormally overexpressed, which significantly enhanced the synthesis of TG and contributed to fatty liver development in mice (Figure 7J).

It is well-established that HFD can induce NAFLD, attributed to HFD consumption leading to microbial dysbiosis, enhancing intestinal permeability, and increasing gut microbiota LPS production.¹⁵ The gut-derived LPS is leaked into the blood and reaches the liver via portal vein. Interestingly, LPS binds to its specific receptors CD14 and TLR4 on Kupffer cells, and then the NF- κ B pathway is activated, which induces the inflammatory factors release and causes hepatic steatosis, even the formation of NAFLD.^{16,17} However, previous studies revealed that low-dose LPS infusion in mice fed with chow diet developed the phenotypes of obesity, insulin resistance, and hepatic steatosis similar to HFD-fed mice.¹⁰ Similarly, another study found that infusion of a low concentration of LPS for 4 weeks could increase liver TG content even in mice fed with chow diet,⁹ suggesting LPS alone might be a key regulator of energy homeostasis, including lipid metabolism. This study supported the findings that low-grade LPS promoted liver steatosis (Fig 1G–H) in mice fed with chow diet. LPS also stimulated lipogenesis in oleic acid preincubated hepatic cells (Figure 3A–D). These data confirmed the previous conclusion that LPS is a regulator of lipid homeostasis and could facilitate the synthesis of TG in the liver.

A rapid augment of proofs shows that individual lifestyle and living conditions can impact the pattern of gene expression through epigenetic modifications, ultimately leading to changes in cellular and tissue behavior and phenotype.^{18,19} DNA methylation is closely correlated with NAFLD pathogenesis.^{20,21} There is an increasing consensus that the DNA methylation profiles are aberrant in patients with NAFLD based on their liver biopsy samples. Clinic-based research showed that the whole DNA methylation in the liver was significantly higher in control overweight participants without NAFLD ($n = 18$) than in patients with NAFLD ($n = 47$).²² The DNA methylation status of lipid metabolism-related genes was also changed in patients with NAFLD. For example, ACLY (ATP citrate lyase) which could promote TG synthesis, was associated with hypomethylation and highly expressed in livers from patients with NAFLD.²³ Mice models of HFD-induced fatty liver revealed a potential relationship between hypomethylation and increased mRNA

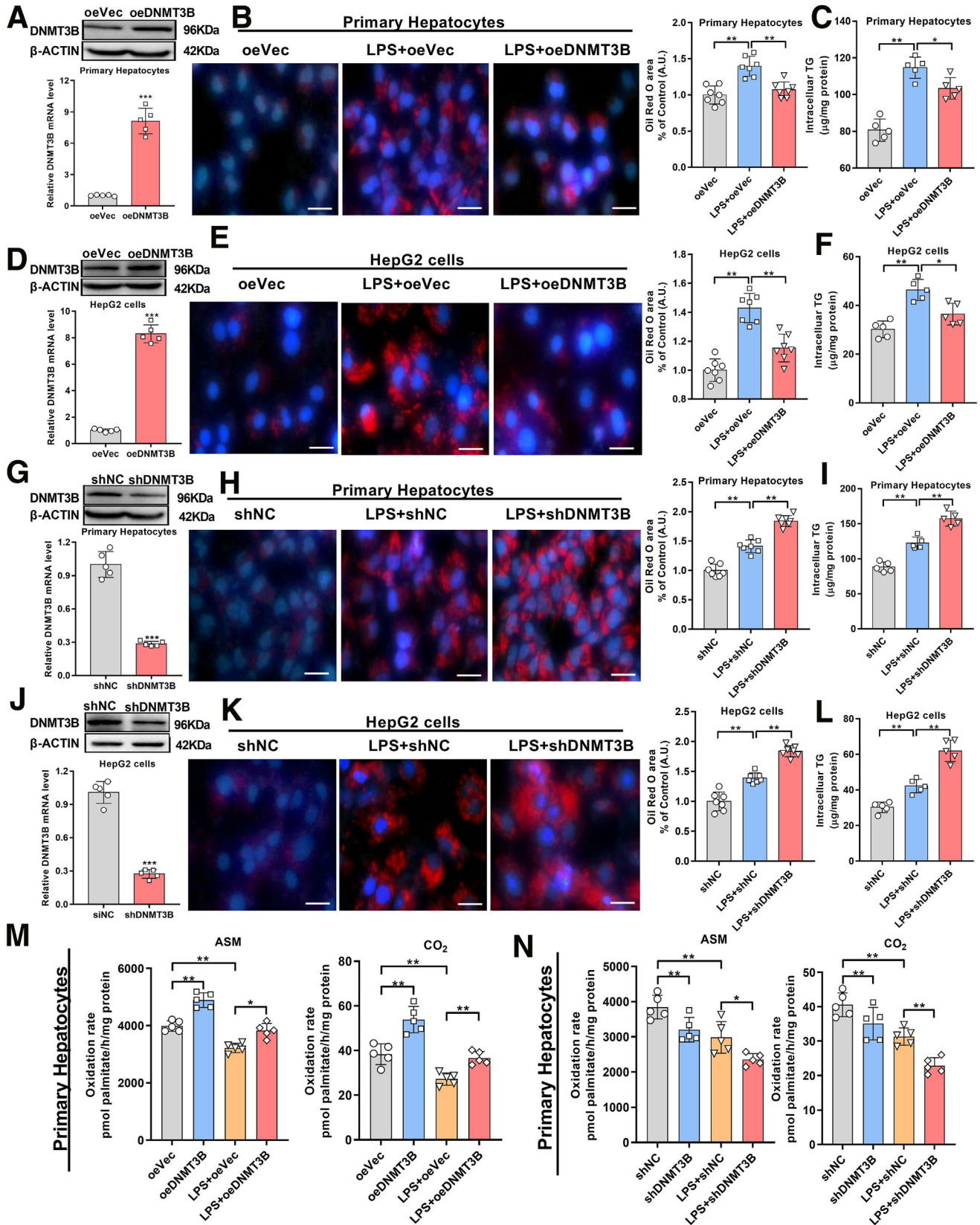
level of the lipogenic gene Apolipoprotein A4 (APOA4).¹³ Because LPS can reportedly alter the DNA methylation pattern in the liver,²⁴ it is highly conceivable that LPS can regulate lipid metabolism through DNA methylation modification of lipogenic genes. This study outlines the potential mechanism by which LPS induces hepatic steatosis. We corroborated that LPS attenuated DNA methylation (Figure 5D–E) via decreasing DNMT3B expression (Figure 3F–H). The lower DNMT3B expression hypomethylated the promoter of lipogenic gene CIDEA (Figure 5F–H) and activated its transcription (Figure 5I) as well as expression (Figure 6D), whereas these effects were reversed after DNMT3B overexpression (Figure 6C, 6E–H). However, how LPS inhibits DNMT3B expression remains to be determined.

LDs are formed by a lipid core encompassed with proteins and a monolayer of phospholipids and are regarded as dynamic metabolic organelles.²⁵ The surface proteins of LDs are mainly divided into 2 types.^{26,27} One is the ER bilayer proteins, including TG biosynthetic enzymes such as DGAT2 and GPAT.^{24,28} The other is the cytosolic proteins comprising PLINs and CIDE.^{29,30} Many studies have shown that the aberrant expression of these proteins could lead to dysbalanced LD synthesis and hydrolysis and then activate the pathogenetic pathway of steatosis in the liver.³¹ For instance, the CIDEA family member CIDEA has been reported to respond to dietary fatty acids and facilitate LDs accumulation and hepatic steatosis development.³² Here, we found CIDEA is the target of LPS-induced hepatic steatosis. LPS significantly increased CIDEA expression in hepatic cells (Figure 5A) and the liver (Figure 7H). Knockdown of CIDEA mitigated the effect of LPS on upregulating hepatic lipid formation (Figure 5K) and prevented further exacerbation of DNMT3B interference on LPS-induced hepatic steatosis (Figure 6I–J). Our data substantiated that CIDEA could be a sensor and mediator of fatty acids caused by hepatic steatosis. Interestingly, malnourished children, patients with anorexia nervosa, and people who lose weight quickly are prone to develop fatty liver, given that hepatocytes accumulate numerous LDs in response to starvation.^{33,34} However, this phenomenon can be ameliorated by a high-protein dietary intervention.³⁵ Recent research has revealed that the essential amino acids of leucine and isoleucine supplements could induce the polyubiquitination and degradation of PLIN2, then inhibit the formation of LDs and decrease the lipid content in the liver.³⁶ Our study consistently showed that LPS upregulated the expression of LD formation-related genes PLIN2, PLIN4, CIDEA, and CIDEA in the liver

Figure 3. (See previous page). LPS promotes lipogenesis in oleic acid-pretreated cells. (A) After 100 μ M oleic acid pretreatment for 24 hours, the Oil Red O staining of LPS (500 ng/mL) or oleic acid (100 μ M) or LPS (500 ng/mL) plus oleic acid (100 μ M)-treated primary hepatocytes were captured. (B) The intracellular TG content was measured ($n = 5$). (C) After oleic acid (100 μ M) pretreatment for 24 hours, the Oil Red O staining of LPS (500 ng/mL) or oleic acid (100 μ M) or LPS (500 ng/mL) plus oleic acid (100 μ M) treated HepG2 cells were obtained. (D) The intracellular TG content was also determined ($n = 5$). (E) Effect of LPS (500 ng/mL) on the mRNA levels of lipid metabolism-related genes ($n = 5$). (F) Heatmap of significantly different expression of RNAs in mice which infused with or without LPS (500 ng/mL) ($n = 3$). (G–H) LPS (500 ng/mL) decreased DNMT3B expression in a dose-dependent manner in hepatic cells ($n = 5$). (I) DNMT3B expression was analyzed in liver samples of healthy, obese, NAFLD, and NASH individuals from Gene Expression Omnibus microarray profiles. Values are determined by the Student t -test when the 2 groups were compared. For 3 or more groups comparison, 1-way analysis of variance followed by Newman-Keuls multiple comparison test was used. Data are exhibited as mean \pm standard error of the mean. * $P < .05$; ** $P < .01$; *** $P < .001$.

(Figure 1K, Figure 3E). Besides, as shown in Figure 3I, the leaked LPS from the gut is a driver of fatty liver disease via DNMT3B, suggesting that the pathway in this study might

not matter in human NAFLD and NASH. These data indicate the metabolic balance of LDs is critical for non-HFD-induced hepatic steatosis, which LPS can induce.



There are currently no effective and reliable therapeutic strategies for NAFLD. Herein, we provide compelling evidence that the LPS/DNMT3B/CIDEA axis may be a valid diagnostic and therapeutic target for hepatic steatosis. Moreover, we found that tail vein injection of AAV8-DNMT3B effectively decreased serum AST and ALT levels (Figure 7D), protected against LD accumulation (Figure 7E–F), and ameliorated hepatic inflammation (Figure 7G) induced by LPS in mice liver and even in HFD-treated mice. These results raise the possibility that screening existing drugs that increase DNMT3B expression are a promising treatment approach for hepatic steatosis. Besides, considering that LPS alone could trigger LD accumulation in the liver, more emphasis should be placed on high plasma LPS circulation levels even when hepatic steatosis has not yet developed. Dietary supplements or medications that can alleviate endotoxemia may be a viable therapeutic strategy for addressing this condition.

To summarize, our study confirms the role of LPS in promoting lipogenesis in the liver, which has been revealed by previous studies. Mechanistically, LPS exacerbates hepatic steatosis by reducing DNMT3B expression and DNA methylation in CIDEA promoter region, which activates the transcription and expression of CIDEA. Targeting DNMT3B expression represents a promising therapy for hepatic steatosis. These findings could broaden the molecular mechanisms understanding that contributing to LPS-induced liver steatosis.

Methods

Animal Experiment

Five-week-old C57BL/6J mice (male, weighing 15–17 g) were obtained from Chang Zhou Cavens Laboratory Animal Ltd, housed at 24 ± 1 °C with 12-hour dark-12-hour light cycle. Mice were free to water and food. After acclimation (1 week), mice were fed either with chow diet (kcal fat 10%) or HFD (kcal fat 60%) for 8 weeks. Mice were sacrificed after 12-hour overnight fasting, then blood and tissue samples were gathered. Some of liver tissues were fixed with paraformaldehyde (4%), whereas the remaining were frozen immediately in liquid nitrogen.

For LPS treatment, the micro-osmotic pumps (Alzet Model 1002) were subcutaneously implanted in mice as previously described.³⁷ LPS (*Escherichia coli* 055:B5, Sigma-Aldrich) at a dose of 300 µg/kg/day or 0.9% NaCl were

filled in pumps and then infused for 4 weeks. Pumps were moved gently every day to avoid adhesion.

At the 7th week and after 6-hour fasting, the OGTT was conducted. Glucose solution was given to mice by oral gavage (2 g/kg). Blood samples were gathered every 30 minutes from caudal vein. The glucometer (Bayer Contour) was employed for blood sugar detection.

For adeno-associated virus (AAV) infection, AAV8 (HANBIO Biotechnology Co, Ltd), which has a strong liver tropism in mice, was used. Mice received a vena caudalis injection of 100 µl AAV-DNMT3B (1×10^9 TU/mL) or AAV-GFP (1×10^9 TU/mL) 1 week before receiving a chow diet or HFD feed for 8 weeks. Sample collection was conducted as previously mentioned.

The Institutional Animal Care and Use Committee of Bengbu Medical College has authorized our animal study (reference no.2021LDK141), and we strictly complied with the institutional guidelines during the process of experiment.

Histological Analysis

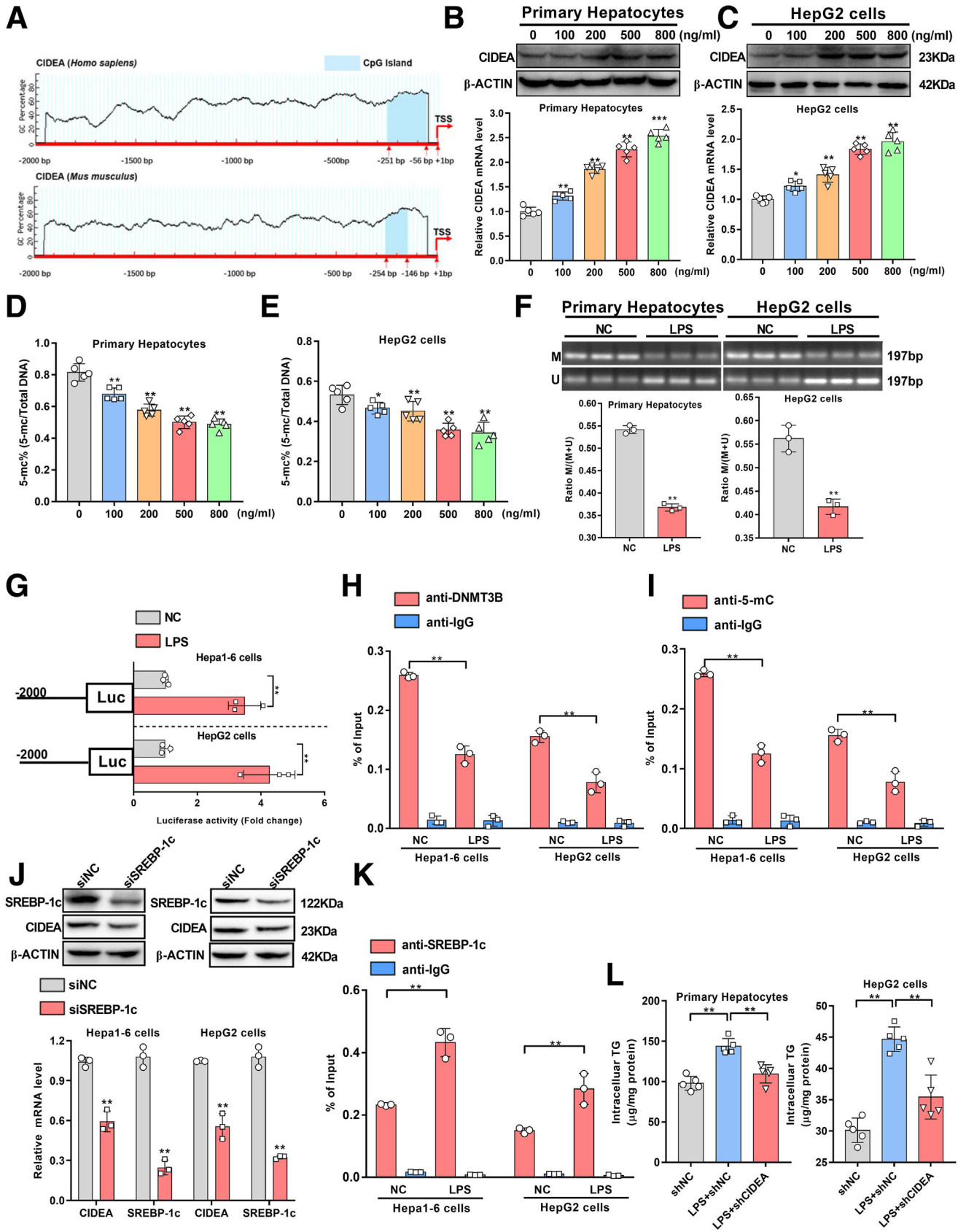
For Sirius red or hematoxylin and eosin (H&E) staining, the fresh liver tissues fixed with 4% formaldehyde were dehydrated by 70%, 80%, and 90% alcohol separately and then embedded in paraffin. Sections about 5-µm thick were cut and stained with Sirius red or H&E (Beyotime).

For Oil Red O dyeing, the frozen liver tissue sections (5 µm-thick) were obtained and dyed with filtered Oil Red O (Solarbio). Samples were counterstained with H&E after washing and finally mounted in glycerin jelly.

Inflammation Biomarker Preparation

The quantification of inflammation biomarkers including G-CSF, IL-10, IL-13, IFN γ , IL-2, TNF α , IL-17A, IL-12p70, IL-4, IL-1 β , MCP-1, IL-23p19, and IL-6, were performed by using a custom RayPlex Human Multiplex Bead Array kit (FAH-INF-1-96). Generally, 100 mg of liver tissue was lysed, and samples were centrifuged to obtain the liquid phase. Twenty-five µl of diluted liquid phase was added into the beads, which were treated per the manufacturer's instructions. Then the beads were shaken at 1000 rpm for 2 hours at room temperature. Beads were incubated and then rinsed for the subsequent flow cytometric analysis. The values of PE MFI were acquired to calculate the concentration of each biomarker from standard curves.

Figure 4. (See previous page). Induction of DNMT3B expression inhibits lipogenesis in LPS-treated hepatic cells. Hepatic cells were co-cultured with lentiviruses (expressing DNMT3B or DNMT3B shRNA) and the corresponding control fragments. (A) The overexpression efficiency of DNMT3B in primary hepatocytes. (B–C) Oil Red O and TG content measurement of oleic acid (100 µM) preincubated primary hepatocytes with DNMT3B overexpression and LPS (500 ng/mL) treatment (n = 5). (D) Efficiency of DNMT3B overexpression, (E–F) Oil Red O and TG content in HepG2 cells (n = 5). (G) The interference efficiency of DNMT3B siRNA in primary hepatocytes. (H) Oil Red O and TG content detection of oleic acid (100 µM) preincubated primary hepatocytes with DNMT3B knockdown and LPS (500 ng/mL) treatment (n = 5). (J) Efficiency of DNMT3B knockdown, (K–L) Oil Red O and TG detection in HepG2 cells (n = 5). (M) Palmitate oxidation rate (partial and complete oxidation) in primary hepatocytes with LPS (500 ng/mL) treatment and DNMT3B overexpression. (N) Palmitate oxidation rate in HepG2 cells after LPS treatment and DNMT3B inhibition (n = 5). Values are determined by the Student *t*-test when the 2 groups were compared. For 3 or more groups comparison, 1-way analysis of variance followed by Newman-Keuls multiple comparison test was used. Data are exhibited as mean \pm standard error of the mean. **P* < .05; ***P* < .01; ****P* < .001. ASM, Acid-soluble metabolites; siRNA, small interfering RNA.



Non-targeted Metabolomics Analysis

UPLC-MS/MS-based sequencing of metabolin was handled by Biomarker Technologies. In brief, 300 μ L acetonitrile and methanol (1:1, vol/vol), which are pre-cooled, were added to a 30-mg liver sample and homogenized in a grinding miller (60 Hz, 2 minutes). The internal standard of L-2-chlorophenyl alanine (0.2 mg/mL) was added to the mixtures. Mixtures were placed on ice, followed by ultrasonication, and then stored for 30 minutes at -20°C . Supernatant was then added into a sample vial for evaporation. The dried samples were dissolved in pre-cooled acetonitrile and methanol (1:1, vol/vol) and percolate with 0.22 μ m filtering membrane for UPLC-MS/MS detection. The data were analyzed by QI 2.3, and the general spectral intensity was facilitated for standardization.

P -value $< .05$, VIP > 1 , fold change ≤ 0.5 , or fold change ≥ 1.5 were used as the cutoff criteria for differentially expressed metabolites between the 2 groups. Data were imported into ClustVis (<https://biit.cs.ut.ee/clustvis/>) for principal component analysis. The SIMCA software (MKS Umetrics) was used for orthogonal partial least squares discriminant analysis. The biochemical metabolic pathways enrichment was processed via KEGG (<https://www.kegg.jp/>). Pathway topology analysis was performed by Metabo Analyst (<https://www.metaboanalyst.ca/>).

Serum Samples Biochemical Analysis

The whole trunk blood was collected after mice were sacrificed and centrifuged for 10 minutes (4°C at 3000 rpm). Supernatant was obtained as the serum. For LPS detection, the Tachypleus Amebocyte Lysate (TAL) assay was used. Briefly, serum samples were diluted 20-fold by distilled water and stored at 70°C for 10 minutes. The TAL reagent purchased from Chinese Horseshoe Crab Reagent Manufactory (EC80545) was dropped following the manufacturer's instructions, and the LPS concentration was determined at absorbance of 545 nm.

The mouse AST ELISA kit (CSB-E12649, CUSABIO) and ALT ELISA kit (CSB-E16539, CUSABIO) were used for AST and ALT measurement (absorbance, 450 nm). For TG and TC measurement, the commercial TG (A110-1) and TC (A111-1) kits (Nanjing Jiancheng) were used. The absorbance was 546 nm and 500 nm, respectively. All the procedures are per the manufacturers' instructions.

Hepatic Primary Cells Isolation and Culture

Tissue primary hepatocytes were obtained as previously stated.¹⁵ Briefly, male C57BL/6 wild-type mice were anesthetized with isoflurane. The inferior vena cava was inserted with a catheter and perfused with preheated D-Hanks solution at 37°C for 10 minutes. Fifty mg/mL type I collagenase (YEASON) was perfused (1.5 mL/min). The liver tissues were disaggregated gently, then incubated with 0.02% collagenase for 15 minutes at 37°C . The supernatant liquid was collected and filtered with 80- μ m nylon mesh, then centrifuged at 4°C for 5 minutes. Isolated hepatocytes were inoculated (1×10^5 cells for 6-well plate), supplemented with 10% fetal bovine serum, and grown with penicillin-streptomycin combination antibiotics. When cells reached 80% confluence, the following assays were performed.

Cell Lines, Culture

HepG2 and Hepa1-6 were got from Cell Bank of Chinese Academy of Sciences. Both cell lines have DNA fingerprinting authentication. All cells were cultured in CO_2 incubator and supplemented with DMEM medium (10% fetal bovine serum, penicillin-streptomycin antibiotics).

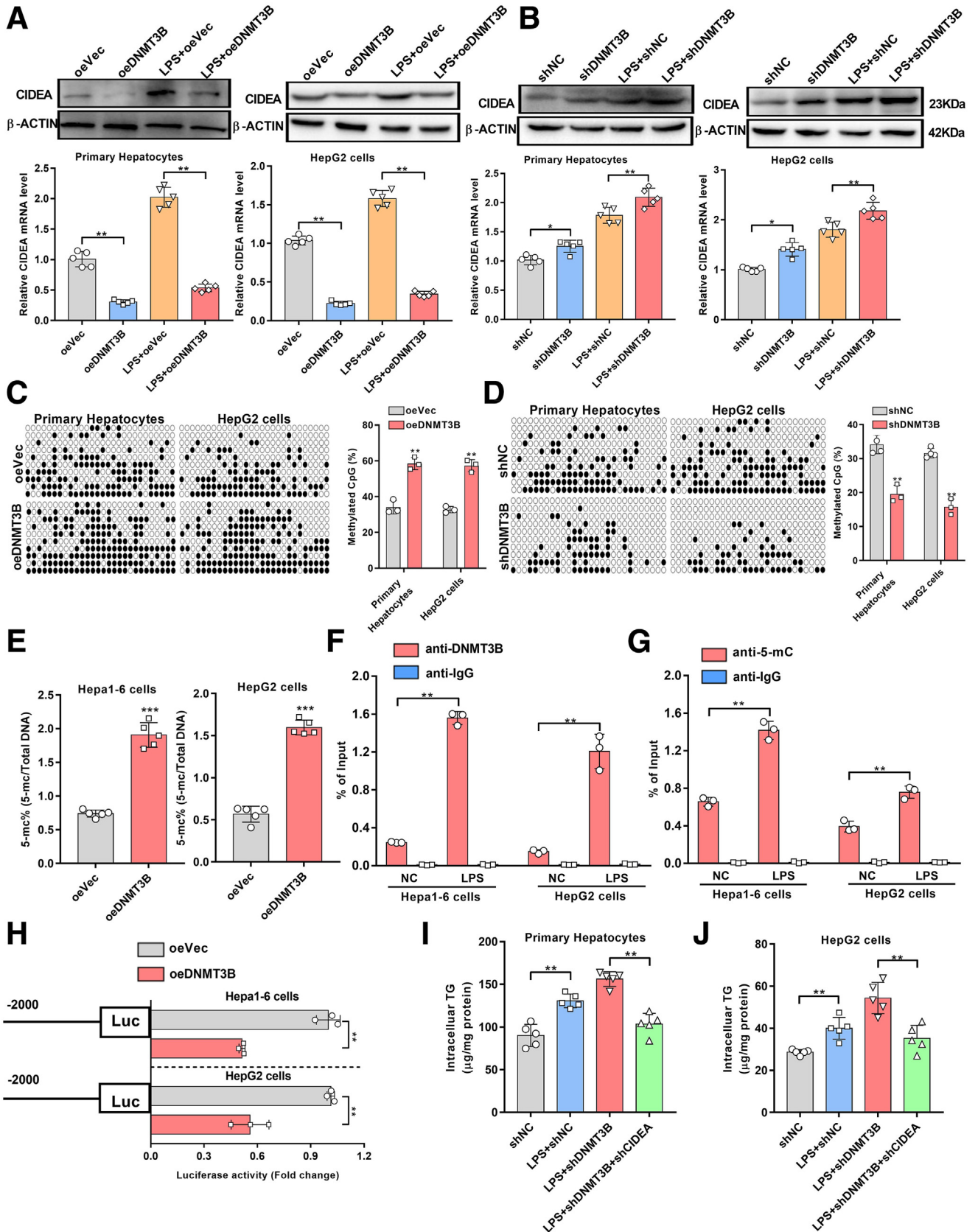
Proliferation Assay

For cell viability assay, the 96-well plates were inoculated with cells (1000 for every well). Cells were incubated with LPS (0, 100, 200, 500, 800 ng/mL for HepG2 cells and 0, 10, 20, 50, 100 ng/mL for primary hepatic cells) for 24 hours and then measured by CCK-8 (Beyotime) at different time points (0 hours and 24 hours; absorbance, 450 nm). The concentration of LPS, which did not affect cell viability, was used for further cell treatment.

Plasmid Construction, siRNA Constructs and Transfection

For the construction of overexpression (OE) plasmids, CDS of human DNMT3B (NM_001207055.2) and mouse DNMT3B (NM_001003960.4) were constructed into vector pcDNA 3.1 (+) by Sangon Biotech. The pcDNA 3.1 (+) was used as a control (a kind gift from Dr Chen). For the siRNAs constructs, the siRNAs were bought from RiboBio. Both OE plasmids and siRNAs were transfected into the HepG2 or Hepa1-6 cells by Lipo8000 Transfection Reagent

Figure 5. (See previous page). LPS facilitates CIDEA expression by demethylating its promoter. (A) Data from the Meth Primer site predicted the CpG islands' location in the CIDEA promoter (*Homo sapiens* and *Mus musculus*). (B–C) Effect of LPS on CIDEA expression in a dose-dependent manner in hepatic cells ($n = 5$). (D–E) Different concentrations of LPS affected the total 5-mC levels in hepatic cells ($n = 5$). (F) Representative methylation-specific PCR (MSP) showed the methylation status of CIDEA CpG island after LPS (500 ng/mL) treatment in primary hepatocytes and HepG2 cells. Ratio (M/M+U) represents the methylated rate ($n = 3$). (G) LPS (500 ng/mL) affects the transcription activity of CIDEA ($n = 3$). (H–I) Quantitative ChIP reveals the enrichment of DNMT3B within the predicted region in LPS (500 ng/mL)-treated hepatocytes ($n = 3$). (J) Effect of SREBP-1c interference on CIDEA expression ($n = 3$). (K) The levels of SREBP-1c binding at the promoter of CIDEA in LPS (500 ng/mL)-treated hepatocytes ($n = 3$). (L) Effect of CIDEA knockdown with lentivirus expressing shRNA on LPS (500 ng/mL)-induced TG accumulation in primary hepatocytes and HepG2 cells pretreated with oleic acid (100 μ M) ($n = 3$). Values are determined by the Student t -test when the 2 groups were compared. For 3 or more groups comparison, 1-way analysis of variance followed by Newman-Keuls multiple comparison test was used. Data are exhibited as mean \pm standard error of the mean. * $P < .05$; ** $P < .01$; *** $P < .001$. 5-mC, 5-methylcytosine; siRNA, small interfering RNA.



(Beyotime). The fragments were also constructed for lentiviruses transfection.

Lipids Content Quantification

Hepatic TG was extracted as documented in previous studies.³⁸ Generally, 100 mg of liver tissue was added to chloroform-methanol (2:1, vol/vol), homogenized in ice for 5 minutes, then shaken at 4 °C for at least 3 hours. Samples were centrifuged after ddH₂O addition to obtain the organic phase. The organic solvent was dried overnight in the fume cupboard, and the TG content was measured.

For cell TG detection, Hepa1-6 and HepG2 cells co-cultured with 100 μM oleic acid bound with BSA (2:1, molar ratio) for 24 hours to stimulate lipid accumulation. Cells were transfected and treated with LPS or extra 100 μM oleic acid or vehicle for 48 hours, then TG content in cell lysates were measured.

For Oil Red O staining, 4% paraformaldehyde was employed to fix cells before staining (Solarbio). After phosphate buffered saline washing and DAPI counterstaining, images of cells were acquired with the Olympus IX53 fluorescence microscope and quantified by ImageJ software.

Fatty Acid Oxidation

The rate of fatty acid oxidation was evaluated by monitoring ¹⁴CO₂ releasing (complete oxidation) and production of ¹⁴C labeled acid-soluble metabolites (incomplete oxidation) mentioned before.³⁹ Generally, cells were cultured in medium including 0.2 mM palmitate, 0.5 μCi/mL (1-¹⁴C)-palmitate (NEC534050UC, Perkin Elmer Inc) and 80 μM BSA. Medium supernatant was then transferred into Whatman filter paper soaked with 0.1 M NaOH covered tube. After addition of 3 M perchloric, the released CO₂ would concentrate on covered paper. The remaining mixture was centrifuged (21,000 g for 10 minutes), and the liquid phase was kept. The radioactivity of acid-soluble metabolites (liquid phase) and CO₂ (cover paper) was measured by a scintillation counter and normalized with protein concentration.

RNA Isolation and Analysis

Total RNA was withdrawn by TRIzol (Invitrogen). RNA (1 μg) was then converted to cDNA (Biyotime). Levels of RNA were confirmed by the RealStar Green Fast Mixture (Genstar) and qRT-PCR in triplicates. β-actin acted as an endogenous control. The primers are listed in Table 1.

Western Blot Assay

Protein extraction from cells or tissues was performed using RIPA Lysis Buffer (with 1% PMSF). Total protein (30 μg) was loaded to SDS-PAGE for electrophoresis. Then proteins were shifted to PVDF membranes (Millipore) for further blocking by skim milk (5% dissolved in TBST). After overnight incubation (4 °C) with antibodies against DNMT3B (ab2851, Abcam, 1:1000), human CIDEA (ab62343, Abcam, 1:1000), mouse (ab8402, Abcam, 1:1000) CIDEA, and β-actin (66009, Proteintech, 1:1000), membranes were rinsed and placed into HRP-conjugated secondary antibodies (Beyotime). The membrane was developed by the BeyoECL Plus kit (Biyotime) and then captured by the ChemiDoc XRS system (Bio-Rad).

DNA Methylation Analysis

Total genomic DNA was extracted by TIANcombi DNA lyse kit (KG203, TIANGEN). For DNA 5-mC measurement, the 5-mC Quantification Kit (P-1034, Epikwik) was employed in accordance with manufacturer's instructions. The 5-mC levels were quantified colorimetrically by reading the absorbance at 450 nm of each well and calculated based on the standard curve.

The potential CpG islands before the gene transcription start site in the DNMT3B promoter region (2000 nucleotides) were predicted using the publicly available online tool MethPrimer (<http://www.urogene.org>). One potential CpG island (-251 to -56bp) was found within the human DNMT3B promoter, and one potential CpG island (-254 to -146bp) within the mouse DNMT3B. The DNA methylation assay was performed as follows. After LPS treatment, genomic DNA from HepG2 and Hepa1-6 cells was obtained. Then, the bisulfite conversion of purified genomic DNA was conducted via Bisul Flash DNA Modification Kit (P-1026, Epikwik) and subjected to methylation-specific PCR using Methylamp MS-qPCR Fast Kit (P-1028, Epikwik) with specific primers (Table 1) designed by the online tool MethPrimer. All the procedures mentioned above were conducted following the manufacturer's instructions.

Chromatin Immunoprecipitation Assay

The ChIP was performed by facilitating ChIP Kit (P2078, Beyotime). Briefly, 1% formaldehyde was used to cross-link HepG2 and Hepa1-6 cells treated with LPS or transiently transfected with pcDNA 3.1 (+) empty vector or DNMT3B overexpression vector. Then cells were sonicated to output DNA fragments about 200–1000bp on a water/ice mixture.

Figure 6. (See previous page). DNMT3B is required for CIDEA expression. (A–B) Effect of DNMT3B overexpression (A) or DNMT3B knockdown (B) on CIDEA expression levels in primary hepatocytes and HepG2 cells (n = 3). (C–D) The CpG islands were detected through bisulfate sequencing (BSP) in the CIDEA promoter region (between -56 and -251bp, -146 and -254 bp from the transcription start site) after DNMT3B overexpression or knockdown. (E) The total 5-mC levels after DNMT3B overexpression (n = 5). (F–G) Quantitative ChIP analysis was used to measure the binding of DNMT3B (F) and 5-mC signals (G) at the promoter of CIDEA in DNMT3B forced expression hepatocytes (n = 5). (H) The transcription activity of CIDEA was verified after DNMT3B overexpression (n = 5). (I–J) Effect of CIDEA interference on TG content in LPS (500 ng/mL)-treated and DNMT3B knockdown hepatic cells that were pretreated with oleic acid (100 μM) for 24 hours (n = 5). Values are determined by the Student *t*-test when the 2 groups were compared. For 3 or more groups comparison, 1-way analysis of variance followed by Newman-Keuls multiple comparison test was used. Data are exhibited as mean ± standard error of the mean. **P* < .05; ***P* < .01; ****P* < .001. 5-mC, 5-methylcytosine; siRNA, small interfering RNA.

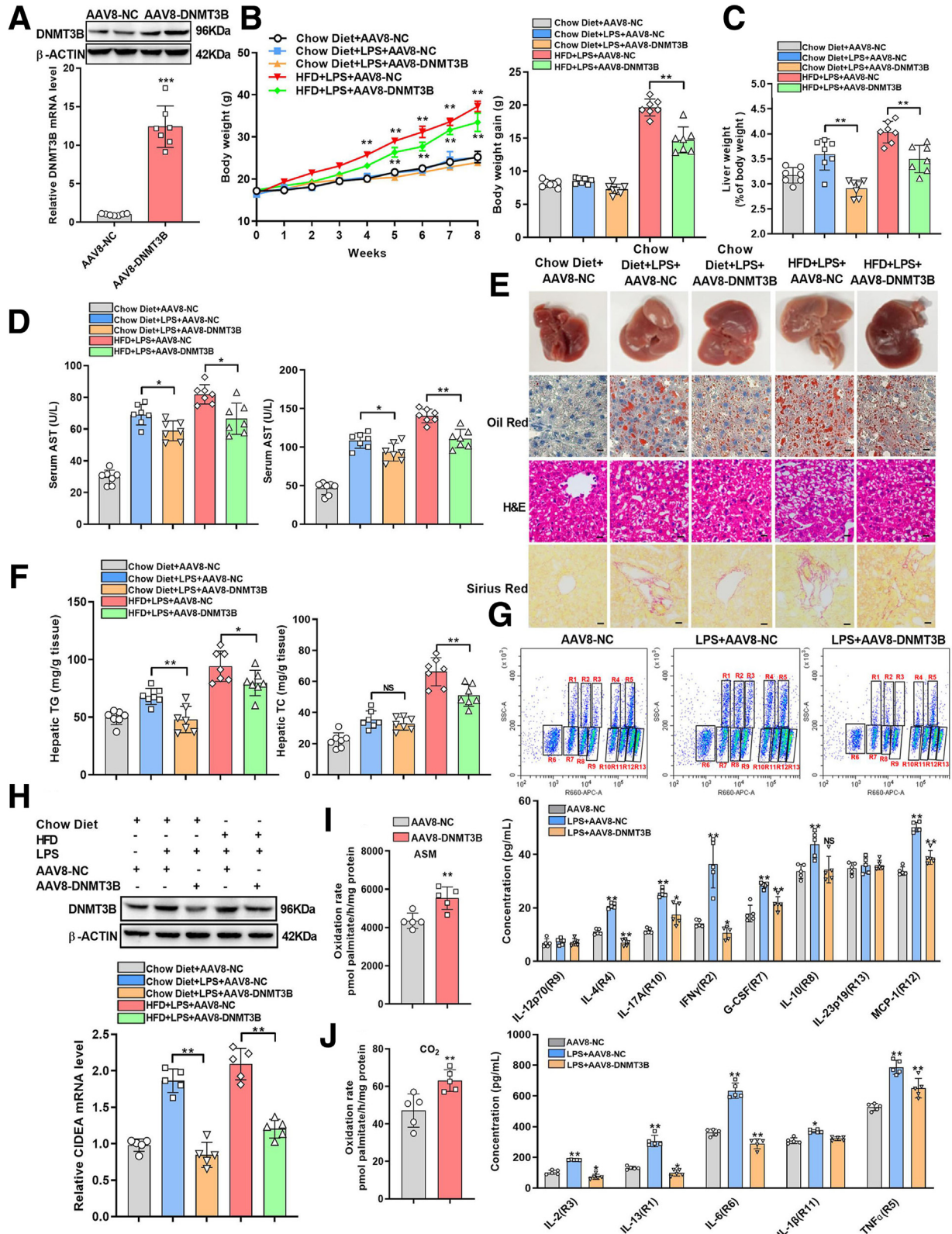


Figure 7. DNMT3B overexpression decreases hepatic steatosis in LPS-infused and HFD-fed mice. C57BL/6 mice (male) were infected with AAV8-DNMT3B or a negative control via tail vein. Chow diet or HFD was then fed to mice for 8 weeks and infused with LPS (300 μ g/kg/day) continuously during the first 4 weeks. (A) Expression efficiency of DNMT3B in mice liver. Body weight (B), liver weight (C), ALT and AST serum level (D) (n = 7). (E) Gross liver appearance (upper), Oil Red O (middle), H&E (middle), Sirius red staining (bottom), and (F) TG content measurement in the indicated group (n = 7). (G) Liver of inflammatory biomarkers (n = 5). (H) Effect of AAV8-DNMT3B on CIDEA expression level in the liver (n = 5). (I–J) Palmitate oxidation rate in hepatocytes isolated from mice liver with AAV8-DNMT3B infection (n = 5). Values are determined by the Student *t*-test when the 2 groups were compared. For 3 or more groups comparison, 1-way analysis of variance followed by Newman-Keuls multiple comparison test was used. Data are exhibited as mean \pm standard error of the mean. ASM, Acid-soluble metabolites.

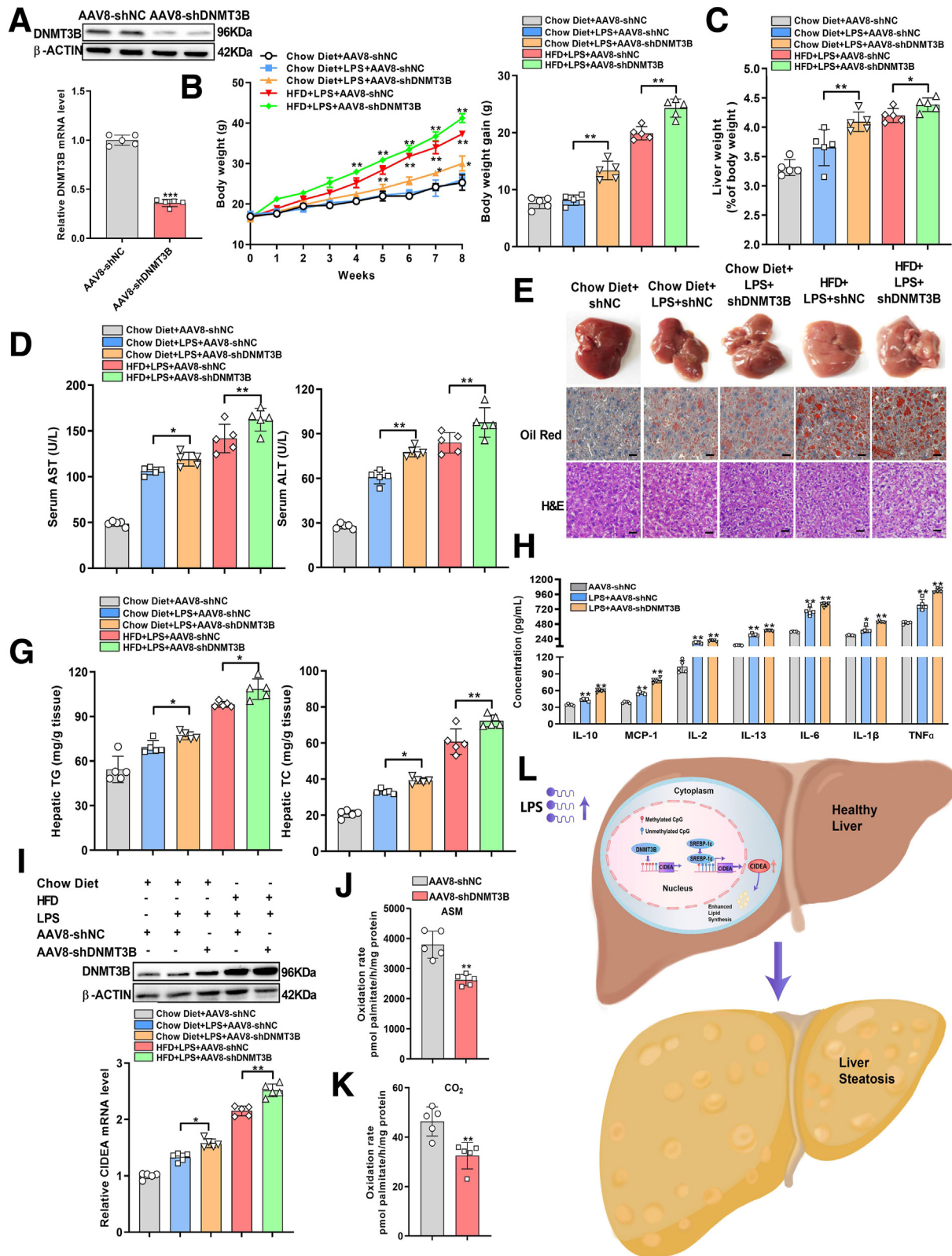


Figure 8. Knockdown increases hepatic steatosis in LPS-infused and HFD-fed mice. C57BL/6 mice (male) were infected with AAV8-shDNMT3B or a negative control via tail vein. Chow diet or HFD was then fed to mice for 8 weeks and infused with LPS (300 $\mu\text{g}/\text{kg}/\text{day}$) continuously during the first 4 weeks. (A) Interference efficiency of DNMT3B in mice liver. Body weight (B), liver weight (C), ALT and AST serum level (D) ($n = 5$). (E) Gross liver appearance, Oil Red O, H&E, and (F) TG content measurement in the indicated group ($n = 7$). (H) Liver of inflammatory biomarkers ($n = 5$). (I) Effect of AAV8-shDNMT3B on CIDEA expression in the liver ($n = 5$). (J-K) Palmitate oxidation rate in hepatocytes isolated from mice liver with AAV8-shDNMT3B infection. (L) The mechanism of LPS/DNMT3B/CIDEA in regulating hepatic steatosis was depicted. Values are determined by the Student t -test when the 2 groups were compared. For 3 or more groups comparison, 1-way analysis of variance followed by Newman-Keuls multiple comparison test was used. Data are exhibited as mean \pm standard error of the mean. * $P < .05$; ** $P < .01$; *** $P < .001$.

Table 1. Primer Sequences List

Primes	Forward (5'-3')	Reverse (5'-3')
ChIP CIDEA Mm	TTTTTTTAAATTTTGTGTTTTTTTT	CTACATACTAAAATCTCCAAAACCC
ChIP CIDEA Hs	TTGTTTAAATTAGGTGGGTTTAGGA	CAAAACCCCTCACTACAAAATAAA
MSP CIDEA Mm M	TATGTTTTTTTTATTTTTTCGACGC	TACATACTAAAATCTCCAAAACCCG
MSP CIDEA Mm U	TGTTTTTTTTATTTTTTGATGTGA	ATACTAAAATCTCCAAAACCCAAC
MSP CIDEA Hs M	TGGTAAGTGATTAAGAGATTCCG	CCGCGAAAACCTAACTAACG
MSP CIDEA Hs U	TGGTAAGTGATTAAGAGATTTGG	CCACAAAACCTAACTAACACA
ChIP SREBP Mm	AGTTTATTAGGTGGTTTTGGGTTT	ACCTCTCTACTCAACAATACCCTCA
ChIP SREBP HS	GGTGGATTTTTGAGTAGGGTTATTT	ACCTAAACATCCAACCTCCCTTTATT
ChIP DNMT3B Mm	TTTAGGTAGTTGGGGGAATATGTAT	CACAACAACCCTACATTAACTTTTTC
ChIP DNMT3B Hs	TTTTTTAAGATGGTTGATAAAGGT	TATAATCACACAACACAAAATCTC
DNMT3B Mm	TGCTGCTGTGCAGTAACACA	ACAACCTGGGTGGCTCAAAT
DNMT3B Hs	CCGCTTCTCGCAGCAG	TCCCTCATGCTTTCCTGCC
FASN Mm	AGATGGAAGGCTGGGCTCTA	GAAGCGTCTCGGGATCTCTG
FASN Hs	TGCAGGAGTTCTGGGACAAC	AATCTGGGTTGATGCCTCCG
SCD1 Mm	GTGCCGTGGGCGAGG	AGCCCAAAGCTCAGCTACTC
SCD1 Hs	GGAGCCACCCTCTTACAAA	AGCCAGGTTTGTAGTACCTCC
SREBP-1c Mm	ACTTTTCCTTAACGTGGGCCCT	TGAGCTGGAGCATGTCTTCG
SREBP-1c Hs	TCCGAGGAACCTTTTCGCCG	CGCCGACTTCACCTTCGAT
DGAT1 Mm	GTAGTGGGCCCAAGGTAGAA	CCTTGCACTACTCAGGATCAGC
DGAT1 Hs	CCTCAGGGTGTCTAGTTCAT	GGGCATTGCTCAAGATCAGC
DGAT2 Mm	AACACGCCCAAGAAAGGTGG	CAGGCATCCGGAAGTTACCA
DGAT2 Hs	TCTGGGAGATGGGGAGTGG	CACCAGCTGGATGGGAAAGT
MOGAT1 Mm	GCAGCCTAATTGGGGCGAA	TTGTACAGGACCAGCATCACC
MOGAT1 Hs	CTTTGACCCATGGCGCCTCT	GTCTGACGAACAGGGATCGG
LIPIN1 Mm	TGCTCGTGAATCCTCTTGAACA	AACCTGTTCCAATGGGCCT
LIPIN1 Hs	CCAGCCTGTGAGAACTAGA	ATTCATGGTCTGCACTCTGCT
MCD Mm	CACGTCCGGGGCATTGT	GGTGAATCCAGGGATAGGCG
MCD Hs	CTCCAGCAACATCCAGGCAAT	TGCTCCTTCGTTTGGCAGTT
LCAD Mm	GTTGCACACATACAGACGGTG	TCCGTGGAGTTGCACACATT
LCAD Hs	TTTTGGGAGGACACCACAGG	GAATGAGAACATCGCGCGGC
UCP2 Mm	AAAGCAGCCTCCAGAACTCC	CTAGCCCTTGACTCTCCCCT
UCP2 Hs	GCCGGCTGGGTCTTATTCTT	GGAACCTCTGCCGAATAGGC
CPT1 Mm	GACTCCGCTCGCTCATTCC	ACCAGTGATGATGCCATTCTTG
CPT1 Hs	GCTTTGGACCGTTGCTGA	CCATGGTCTCCTCCAAGGC
PLIN1 Mm	GACTGAGGTGGCGGTCTG	TTGGCAGCTGTGAACCTGGG
PLIN1 Hs	CGGTCAGCCGACTTG	ACGCCCTTCTCATAGGCATT
CIDEA Mm	GTGAGGGGGAGGTCCAACA	CCATGATGCCTTTGCGAACC
CIDEA Hs	CTGTGAGGGGGAGGTCCAA	CTGGCTTCAGGGTTCCTAhGT
PLIN4 Mm	TCCAAAGGCAAGACCTTGAG	CTGTTCAGAAGGTTGGAGCA
PLIN4 Hs	CTGCCACCCAGAGCAGA	TGGACCACTCCCTTAGCC
Cidea Mm	GACAGAAATGGACACCCGGTA	TGTGCATCGGATGTCGTAGG
Cidea Hs	CTCATCAGGCCCTGACATT	GAGGGCATCCAGAGTCTTGC
PLIN2 Mm	GCTCGGAAGTGCAGCAATG	CTCTCATCACCACGCTCTGT
PLIN2 Hs	GCTGCAGTCCGTGATTTCT	TCTTACACCGTTCTCTGCC
ACC Mm	TCTATCCGTCGGTGGTCT	GCAGTTCTGGGAGTTTCG
ACC Hs	GACCTTAAAGCCAATGCA	TTGAGCCACTATGGAAGA

M, Methylation; U, unmethylation.

Ten percent of each sample was saved as input, whereas the rest was subjected to immunoprecipitation with 2 μ g of antibody specifically against DNMT3B (ab2851, Abcam),

5-mC (ab10805, Abcam). IgG was used as the negative control. After DNA elution and purification, samples were detected by qRT-PCR using specific primers (Table 1).

Promoter Activity Assays

The full promoter region (2000 nucleotides) upstream of the transcription start site in the DNMT3B was constructed and subcloned into PGL 3.0 basic vector by Sangon Biotech. Either vector was co-transfected with DNMT3B over-expression vector or pcDNA 3.1 (+) empty vector into HepG2 or Hepa1-6 cells by Lipo8000 Transfection Reagent (Beyotime). Forty-eight hours after transfection, the Luciferase Reporter Kit (FR201, Transgene) was employed to determine luciferase activities. The firefly luciferase acted as an inner control.

Statistical Analysis

Data sourced from at least 3 replications are shown as mean \pm standard error of the mean. The Student *t*-test is employed for significance analysis in comparison of 2 groups. When 3 or more groups needed to be compared, 1-way analysis of variance with a Newman-Keuls multiple comparison test was adopted. The level of significance was judged when *P* is less than .05. Asterisks denote the significance in all figures (**P* < .05; ***P* < .01; and ****P* < .001).

References

1. Yip TC, Lee HW, Chan WK, et al. Asian perspective on NAFLD-associated HCC. *J Hepatol* 2022;76:726–734.
2. Pang J, Xu W, Zhang X, et al. Significant positive association of endotoxemia with histological severity in 237 patients with non-alcoholic fatty liver disease. *Aliment Pharmacol Ther* 2017;46:175–182.
3. Serfaty L, Lemoine M. Definition and natural history of metabolic steatosis: clinical aspects of NAFLD, NASH and cirrhosis. *Diabetes Metab* 2008;34:634–637.
4. Febbraio MA, Reibe S, Shalpour S, et al. Preclinical models for studying NASH-driven HCC: how useful are they? *Cell Metab* 2019;29:18–26.
5. Woo Baidal JA, Lavine JE. The intersection of nonalcoholic fatty liver disease and obesity. *Sci Transl Med* 2016;8:323rv321.
6. Leung C, Rivera L, Furness JB, et al. The role of the gut microbiota in NAFLD. *Nat Rev Gastroenterol Hepatol* 2016;13:412–425.
7. Ding YY, Fang Y, Pan Y, et al. Orally administered octacosanol improves liver insulin resistance in high-fat diet-fed mice through the reconstruction of the gut microbiota structure and inhibition of the TLR4/NF-kappaB inflammatory pathway. *Food Funct* 2023;14:769–786.
8. Dickerson RN, Karwoski CB. Endotoxin-mediated hepatic lipid accumulation during parenteral nutrition in rats. *J Am Coll Nutr* 2002;21:351–356.
9. Cani PD, Amar J, Iglesias MA, et al. Metabolic endotoxemia initiates obesity and insulin resistance. *Diabetes* 2007;56:1761–1772.
10. Yin Y, Wang Q, Qi M, et al. Ghrelin ameliorates nonalcoholic steatohepatitis induced by chronic low-grade inflammation via blockade of Kupffer cell M1 polarization. *J Cell Physiol* 2021;236:5121–5133.
11. Nano J, Ghanbari M, Wang W, et al. Epigenome-wide association study identifies methylation sites associated with liver enzymes and hepatic steatosis. *Gastroenterology* 2017;153:1096–1106.e2.
12. Eslam M, Valenti L, Romeo S. Genetics and epigenetics of NAFLD and NASH: clinical impact. *J Hepatol* 2018;68:268–279.
13. Kim H, Worsley O, Yang E, et al. Persistent changes in liver methylation and microbiome composition following reversal of diet-induced non-alcoholic-fatty liver disease. *Cell Mol Life Sci* 2019;76:4341–4354.
14. Chen A, Chen X, Cheng S, et al. FTO promotes SREBP1c maturation and enhances CIDEA transcription during lipid accumulation in HepG2 cells. *Biochim Biophys Acta Mol Cell Biol Lipids* 2018;1863:538–548.
15. Ceccarelli S, Panera N, Mina M, et al. LPS-induced TNF-alpha factor mediates pro-inflammatory and pro-fibrogenic pattern in non-alcoholic fatty liver disease. *Oncotarget* 2015;6:41434–41452.
16. Carpino G, Del Ben M, Pastori D, et al. Increased liver localization of lipopolysaccharides in human and experimental NAFLD. *Hepatology* 2020;72:470–485.
17. Kessoku T, Kobayashi T, Imajo K, et al. Endotoxins and non-alcoholic fatty liver disease. *Front Endocrinol (Lausanne)* 2021;12:770986.
18. Portela A, Esteller M. Epigenetic modifications and human disease. *Nat Biotechnol* 2010;28:1057–1068.
19. Mathers JC, Strathdee G, Relton CL. Induction of epigenetic alterations by dietary and other environmental factors. *Adv Genet* 2010;71:3–39.
20. Zeybel M, Hardy T, Robinson SM, et al. Differential DNA methylation of genes involved in fibrosis progression in non-alcoholic fatty liver disease and alcoholic liver disease. *Clin Epigenetics* 2015;7:25.
21. Baumeier C, Saussenthaler S, Kammel A, et al. Hepatic DPP4 DNA methylation associates with fatty liver. *Diabetes* 2017;66:25–35.
22. Lai Z, Chen J, Ding C, et al. Association of hepatic global DNA methylation and serum one-carbon metabolites with histological severity in patients with NAFLD. *Obesity (Silver Spring)* 2020;28:197–205.
23. Ahrens M, Ammerpohl O, von Schonfels W, et al. DNA methylation analysis in nonalcoholic fatty liver disease suggests distinct disease-specific and remodeling signatures after bariatric surgery. *Cell Metab* 2013;18:296–302.
24. Harris CA, Haas JT, Streeper RS, et al. DGAT enzymes are required for triacylglycerol synthesis and lipid droplets in adipocytes. *J Lipid Res* 2011;52:657–667.
25. Mashek DG. Hepatic lipid droplets: a balancing act between energy storage and metabolic dysfunction in NAFLD. *Mol Metab* 2021;50:101115.
26. Jacquier N, Choudhary V, Mari M, et al. Lipid droplets are functionally connected to the endoplasmic reticulum in *Saccharomyces cerevisiae*. *J Cell Sci* 2011;124:2424–2437.
27. Bersuker K, Olzmann JA. Establishing the lipid droplet proteome: mechanisms of lipid droplet protein targeting and degradation. *Biochim Biophys Acta Mol Cell Biol Lipids* 2017;1862:1166–1177.
28. Quiroga IY, Pellon-Maison M, Suchanek AL, et al. Glycerol-3-phosphate acyltransferases 3 and 4 direct

- glycerolipid synthesis and affect functionality in activated macrophages. *Biochem J* 2019;476:85–99.
29. Carr RM, Ahima RS. Pathophysiology of lipid droplet proteins in liver diseases. *Exp Cell Res* 2016;340:187–192.
 30. Barneda D, Planas-Iglesias J, Gaspar ML, et al. The brown adipocyte protein CIDEA promotes lipid droplet fusion via a phosphatidic acid-binding amphipathic helix. *Elife* 2015;4:e07485.
 31. Scorletti E, Carr RM. A new perspective on NAFLD: focusing on lipid droplets. *J Hepatol* 2022;76:934–945.
 32. Zhou L, Xu L, Ye J, et al. Cidea promotes hepatic steatosis by sensing dietary fatty acids. *Hepatology* 2012;56:95–107.
 33. Liebe R, Esposito I, Bock HH, et al. Diagnosis and management of secondary causes of steatohepatitis. *J Hepatol* 2021;74:1455–1471.
 34. Semova I, Biddinger SB. Triglycerides in nonalcoholic fatty liver disease: guilty until proven innocent. *Trends Pharmacol Sci* 2021;42:183–190.
 35. De Chiara F, Ureta Checcllo C, Ramon Azcon J. High protein diet and metabolic plasticity in non-alcoholic fatty liver disease: myths and truths. *Nutrients* 2019;11:2985.
 36. Zhang Y, Lin S, Peng J, et al. Amelioration of hepatic steatosis by dietary essential amino acid-induced ubiquitination. *Mol Cell* 2022;82:1528–1542.e10.
 37. Cani PD, Knauf C, Iglesias MA, et al. Improvement of glucose tolerance and hepatic insulin sensitivity by oligofructose requires a functional glucagon-like peptide 1 receptor. *Diabetes* 2006;55:1484–1490.
 38. Porteiro B, Fondevila MF, Buque X, et al. Pharmacological stimulation of p53 with low-dose doxorubicin ameliorates diet-induced nonalcoholic steatosis and steatohepatitis. *Mol Metab* 2018;8:132–143.
 39. Vila-Brau A, De Sousa-Coelho AL, Mayordomo C, et al. Human HMGCS2 regulates mitochondrial fatty acid oxidation and FGF21 expression in HepG2 cell line. *J Biol Chem* 2011;286:20423–20430.

Received April 2, 2023. Accepted September 5, 2023.

Correspondence

Address correspondence to: Guoquan Liu, PhD, Department of Biochemistry and Molecular Biology, School of Laboratory Medicine, Bengbu Medical College, Donghai Road, Anhui, China. e-mail: 851404957@qq.com; or Qiang Li, PhD, Department of Cell Biology, School of Life Science, Bengbu Medical College, Donghai Road, Anhui, China. e-mail: 2812426235@qq.com.

Acknowledgments

The authors thank Guoquan Liu (Bengbu Medical College) for conducting data analysis of ATAC-seq, genome bisulfite sequencing (BSP), and providing an experimental platform and instruments.

CRedit Authorship Contributions

Qiang Li (Project administration: Lead; Supervision: Equal; Writing – review & editing: Lead)

Wenjing Wang (Data curation: Equal; Formal analysis: Equal; Writing – original draft: Equal)

Feifan Duan (Data curation: Equal; Formal analysis: Equal; Writing – original draft: Equal)

Yaju Wang (Data curation: Equal)

Shuya Chen (Data curation: Equal)

Kangyun Shi (Methodology: Equal; Software: Equal)

Yinyin Xia (Formal analysis: Equal; Software: Equal)

Yu Gao (Supervision: Supporting)

Xinyu Li (Formal analysis: Equal; Software: Equal)

Guoquan Liu (Project administration: Lead; Resources: Lead; Supervision: Lead; Validation: Lead)

Conflicts of interest

The authors disclose no conflicts.

Funding

This work was supported by Anhui Provincial Natural Science Foundation (Grant No. 2108085MH284), the Natural Science Research Project of Anhui Educational Committee (Grant No. KJ2020A0580), and the National Innovation and Entrepreneurship Training Project for University (Grant No.202110367065).